

Thermometric Calibration of the Ultrafast Relaxation Dynamics in Plasmonic Au Nanoparticles

Marzia Ferrera,[†] Giuseppe Della Valle,[‡] Maria Sygletou,[†] Michele Magnozzi,^{¶,†}
Daniele Catone,[§] Patrick O’Keeffe,^{||} Alessandra Paladini,^{||} Francesco Toschi,^{||}
Lorenzo Mattera,[†] Maurizio Canepa,[†] and Francesco Bisio^{*,⊥}

[†]*OptMatLab, Dipartimento di Fisica, Università di Genova, via Dodecaneso 33, I-16146
Genova, Italy*

[‡]*Dipartimento di Fisica, IFN-CNR, Politecnico di Milano, Piazza Leonardo da Vinci 32,
I-20133 Milano, Italy*

[¶]*INFN, Sezione di Genova, via Dodecaneso 33, I-16146 Genova, Italy*

[§]*CNR-ISM, Division of Ultrafast Processes in Materials (FLASHit), Area della Ricerca di
Roma Tor Vergata, Via del Fosso del Cavaliere, 100, I-00133 Rome, Italy*

^{||}*CNR-ISM, Division of Ultrafast Processes in Materials (FLASHit), Area della Ricerca di
Roma 1, I-00015 Monterotondo Scalo, Italy*

[⊥]*CNR-SPIN, C.so Perrone 24, I-16152 Genova, Italy*

E-mail: francesco.bisio@spin.cnr.it

This article may be downloaded for personal use only. Any other use requires prior permission of the author and ACS Publishing. This article appeared in (M. Ferrera, ACS Photonics 2020, 7, 4, 959–966) and may be found at (<https://10.1021/acsphotonics.9b01605>).

Abstract

The excitation of plasmonic nanoparticles by ultrashort laser pulses sets in motion a complex ultrafast relaxation process involving the gradual re-equilibration of the system's electron gas, lattice and environment. One of the major hurdles in studying these processes is the lack of *direct* measurements of the dynamic temperature evolution of the system subcomponents.

We measured the dynamic optical response of ensembles of plasmonic Au nanoparticles following ultrashort-pulse excitation and we compared it with the corresponding static optical response as a function of the increasing temperature of the thermodynamic bath. Evaluating the two sets of data, the optical fingerprints of equilibrium or off-equilibrium responses could be clearly identified, allowing us to extract a dynamic thermometric calibration scale of the relaxation process, yielding the experimental ultrafast temperature evolution of the plasmonic particles as a function of time.

keywords: Plasmonics, Gold Nanoparticles, Ultrafast Dynamics, Thermoplasmonics, Optical Spectroscopy

The irradiation of nanometric metallic particles (NPs) with ultrafast laser pulses sets in motion a time-dependent dynamics that affects the electron gas, the lattice and the local environment of the NPs.¹⁻⁸ Depending on the characteristics of the exciting radiation (fluence, wavelength, pulse duration *etc.*), the NPs may exhibit radically-different time-dependent evolutions, along which intriguing, off-equilibrium states of matter may occur.⁹⁻¹² The typical relaxation pathway of NPs lying within a thermodynamic bath at temperature T_{bath} and impulsively excited by a radiation pulse at $\tau = 0$ can be schematically divided in three distinct steps.^{13,14} First, the radiation pulse induces an out-of-equilibrium electron population that thermalizes *via* e - e scattering at $T_e \gg T_{bath}$ within few 100-fs;¹⁵ then the energy exchange with the NP lattice *via* e - ph coupling leads to the thermalization, on the few- ps time scale, of the NP lattice with the electron gas at $T_e = T_l > T_{bath}$ and, finally, phonon-phonon interactions lead to the thermalization of the NPs with their environment ($T_e = T_l = T_{env}$) over tens to hundreds of ps . The energy dissipation to the thermodynamic bath determines the subsequent, slow asymptotic evolution of the overall temperature towards T_{bath} .

The process outlined above is however far from being straightforward. The photon energy, the radiation fluence F , the NP size¹⁶ and environment,¹⁷ the occurrence of plasmonic resonances and hot-spots¹⁸⁻²⁰ or the hot-electron injection from NPs to their environment^{14,21,22} all play a role in influencing the actual relaxation pathway. Additionally, the electron and lattice heat capacitances, the materials' dielectric functions^{23,24} and the related-interface thermal resistances, exhibit an (often unexplored) temperature dependence. Last but not least, temperature-driven morphological effects can come into play²⁵ and the environment temperature T_{env} may exhibit huge spatial gradients around the NPs on the ps time scale. Given this, it is hardly surprising that understanding and modelling the ultrafast relaxation dynamics of impulsively-excited matter and of plasmonic NPs is a task that remains challenging to this day.^{22,26-35}

Experimentally, the progresses in ultrafast optical and electronic spectroscopies have allowed,

over the years, deeper and deeper insights in these complicated processes,^{35–40} ultimately promoting the emergence of the above-described general picture. One crucial point is however still represented by the fact that, while T_e , T_l and T_{env} are basic ingredients of theoretical models, their evaluation from experimental data is typically always *indirect*.^{41,42}

In this work we report a simple experimental approach that may significantly improve the quantitative understanding of ultrafast dynamics in solid-state systems. We investigated the optical response of ordered arrays of plasmonic Au NPs under two different experimental conditions. First, we recorded their ultrafast optical response following pulsed-laser irradiation, by means of pump-probe transient absorbance spectroscopy (TAS). Then, we measured their *static* optical response as a function of variable thermodynamic-bath temperature, T_{bath} , in a separate experiment.

In the former case, T_e , T_l and T_{env} are complicated functions of the delay time τ elapsed since the exciting pulse. In the latter case, by definition $T_e = T_l = T_{env} = T_{bath}$, where T_{bath} is known. Comparing the ultrafast response with the static data, we were therefore able to ascertain the optical fingerprints of equilibrium or off-equilibrium behaviour and experimentally estimate the delay time for which the intraparticle equilibrium condition ($T_e = T_l$) is achieved. From then onwards, we could follow the temperature-relaxation dynamics, extracting an effective thermometric calibration scale that allowed us to assess the ultrafast temperature evolution of the NP ensembles.

Experimental

The samples consisted of 2D arrays of Au NPs fabricated by solid-state dewetting of ultrathin Au films onto a nanopatterned LiF(110) single crystal. The sample fabrication procedures are described in detail in previous works.^{20,43–45} The system is composed of densely-packed Au NPs (areal density $10^3 \pm 100$ NP/ μm^2), with mean size around 20–25 nm, circular in-

plane cross section and short-range order, laid on a transparent LiF(110) substrate (Crystec GmbH). An atomic-force microscopy image of the system is reported in the Supporting Information (Figure S1). The system exhibits a room-temperature (RT) localized surface plasmon resonance (LSPR) at $\lambda_{LSPR} \approx 560$ nm, as reported in Fig. 1(a) for 293 K.

The static optical response of the NPs as a function of T_{bath} was assessed by means of temperature-dependent optical transmittance spectroscopy (400-800 nm range), performed in a home-designed high-vacuum (HV) vessel ($p < 10^{-7}$ mbar). White light from an incandescence W lamp was collimated, linearly polarized, and directed onto the sample through a transparent stress-free optical viewport (see the Supporting Information (Figure S2)). The transmitted light exited the HV chamber through another viewport and was collected by a spectrometer (Ocean Optics USB2000+). The transmittance spectra were normalized to the bare-substrate response. The lamp intensity decreases at both ends of the spectrum, causing a larger noise level at wavelengths below 450 nm and above 700 nm. Temperature dependent spectra were collected during a decreasing- T_{bath} ramp, starting from the maximum temperature $T_{bath} = 660$ K until RT, in order to limit any spurious influence of weakly-bound contaminants. Upon approaching RT, liquid nitrogen cooling was applied to speed the temperature ramp and limit any unwanted effect due to a prolonged permanence in HV.

The ultrafast, time-resolved measurements were performed by means of TAS. The laser pulses used for exciting/heating and probing of the 2D arrays were produced by a single femtosecond laser system. This system consists of a Ti:Sapphire oscillator delivering 20 fs pulses with a frequency of 80 MHz, a part of whose output is used to seed a chirped pulse amplifier which in turn generates 4 mJ, 35 fs pulses centered at 800 nm with a repetition rate of 1 kHz. An optical parametric amplifier (OPA) is then used to convert part of the amplifier output into tunable radiation. The output of the OPA at a wavelength of 410 nm is used as the pump pulse. The experimental fluence on the sample was $F = (4 \pm 2)$ J/m². The error stems from the uncertainty on the spot diameter dimension (400 ± 100) μ m. For the probe, white light supercontinuum (SC) pulses (350-800 nm) are generated by focusing 3

μJ of the amplifier radiation into a rotating CaF_2 crystal. The latter is used in a split-beam configuration in which 50% of the white light passes through the sample while the remainder is used as a reference to account for pulse-to-pulse fluctuations in the white-light generation. The delay between the two pulses is scanned by varying the optical path of the probe light.⁴⁶ The absence of damage following the laser irradiation was assessed by checking the stability of the sample morphology and optical response. Variations of sample morphology were observed for laser fluences of 13 J/m^2 and above.²⁰

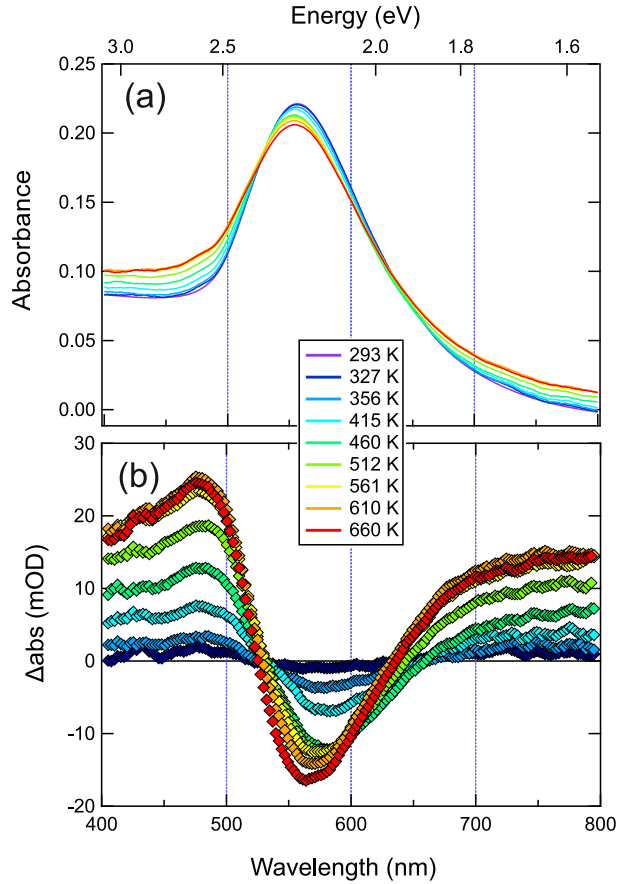


Figure 1: Panel (a): experimental static absorbance spectra of Au NPs as a function of T_{bath} . Panel (b): differential-absorbance spectra relative to room-temperature absorbance, calculated from the data of panel (a).

In Fig. 1(a) we report a set of static absorbance spectra of the Au NPs as a function of T_{bath} ; the peak at $\lambda \approx 560 \text{ nm}$ is the fingerprint of the LSPR of the NP array, red shifted and broadened with respect to the LSPR of the individual NPs because of coupling

effects and inhomogeneities in the array.⁴⁴ As a function of increasing T_{bath} we can observe that the LSPR absorbance peak broadens and weakens, due to the larger optical losses induced by the increased phonon population (plasmon bleaching, PB). The full-width at half maximum of the LSPR peak evolves from 0.46 eV to 0.49 eV from RT to 660 K, similar to previous observations.^{47,48} To better highlight the temperature effects, in Fig.1(b) we report the corresponding differential-absorbance spectra ΔAbs , calculated as $\Delta\text{Abs}(T_{bath}) = \text{Abs}(T_{bath}) - \text{Abs}(293 \text{ K})$. The plasmon bleaching is apparent as the prominent negative feature in the center of the spectral range, whereas positive wings (photo-induced absorption, PIA) arise from the LSPR broadening with increasing T_{bath} . The PB and PIA decrease in magnitude with decreasing temperature, and the PB peak position initially redshifts with increasing T_{bath} , then blueshifts from 415 K onwards. The initial redshift of the PB peak followed by its blueshift are a consequence of the fact that the LSPR peak very slightly blueshifts for T up to 415 K, and then redshifts with increasing T. We believe that the experimental trend of the PB peak reflects two conflicting behaviors, namely a redshift of the LSPR induced by the gradual broadening of the interband transitions of Au with increasing T, and a blueshift due to the temperature-induced shift of the plasma frequency to higher wavelengths.²³ More complex effects depending on the peculiar configuration of the sample, including thermal dilatation and subsequent change in the interparticle coupling, could also contribute to these subtle dispersive features of thermo-modulation spectra, whose precise explanation is beyond the scope of the present study.

In Fig. 2(a),(b) we report the results of TAS measurements performed on the same system. On the horizontal scale is the time delay τ , expressed in *ps*, and on the vertical scale, the probe wavelength. The color scale represents the ΔAbs of the system, expressed in mOD, as the difference between the absorbance of the excited and unperturbed system, respectively. In Fig. 2(a) we report a broad time scan, up to $\tau \approx 300 \text{ ps}$, on a logarithmic time scale, whereas in Fig. 2(b) we focus on the first few *ps* of dynamics. The horizontal dashed line represents the wavelength of the static LSPR maximum at RT. The TAS data

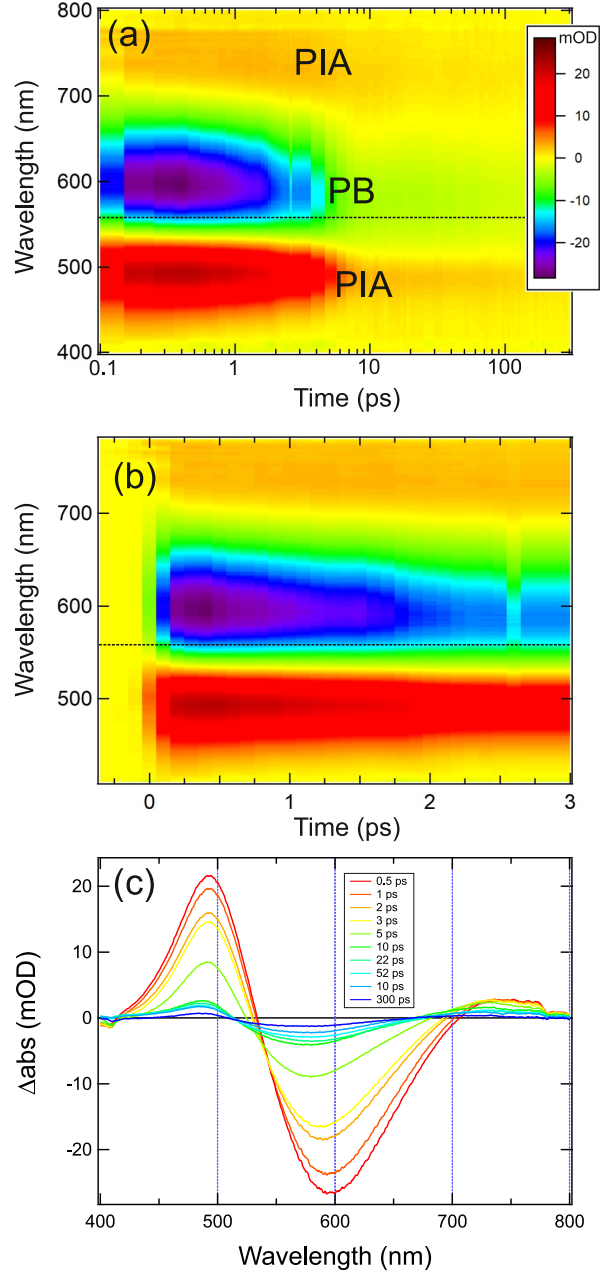


Figure 2: Panels (a), (b): Femtosecond transient-absorbance map of Au NPs. The vertical scale represents the probe wavelength, the horizontal scale the delay time τ elapsed since the 410-nm excitation pulse, on a logarithmic (a), and linear (b) scale, respectively. Panel (c): transient absorbance spectra as a function of time-delay τ , extracted from the map of panels (a), (b).

clearly show the PB feature at $\lambda \approx 595$ nm, accompanied by the PIA on the wings of the LSPR. After a sharp rise in the first few 100 *fs*, all the features fade in intensity with growing τ , in agreement with expectations^{4,32,37} and the PB peak gradually blueshifts, inching closer to the static LSPR wavelength.

In Fig. 2 (c), we report TA spectra (*i.e.* spectral cuts at selected τ), ranging between 0.5 *ps* and 300 *ps*. In those spectra, the PB is apparent as the prominent negative feature at $\lambda \approx 600$ nm, whereas the PIA structures are found around $\lambda \approx 490$ nm (the most intense) and at $\lambda > 700$ nm. Here, we observe that the PB peak monotonously blueshifts as a function of increasing delay.

Discussion

Comparing the two sets of data of Fig. 1 and 2, we can notice that the short-delay intensity of the PB and PIA features in TA spectra matches the static values of PB and PIA intensity retrieved for high- T_{bath} , and analogously so for intermediate-delays/intermediate- T_{bath} and long-delays/low- T_{bath} data. In Fig. 3 we therefore directly compare sets of Δ Abs spectra recorded in the two different experiments. In panel (a) we report short-delay TA spectra ($\tau = 0.5$ *ps* to $\tau = 3$ *ps*) along with high- T_{bath} Δ Abs spectra (460 K to 660 K), while in panels (b), (c) we compare intermediate-delay TA spectra (22 *ps* and 52 *ps*) with static Δ Abs($T_{bath} = 356$ K), and long-delay TA spectra ($\tau = 300$ *ps*) with Δ Abs($T_{bath} = 327$ K), respectively.

The overall spectral shape of the Δ Abs spectra is similar for all data, yet it is apparent that none of the high- T_{bath} *static* spectra can match the short-delay TAS data (Fig. 3(a)). In particular, large discrepancies in the spectral position of the PB peak and of the long- λ zero crossing appear. This clearly underscores the well-known fact that impulsive excitations at ultrashort delays do *not* simply heat the NPs, but create out-of-equilibrium conditions whose optical response cannot be reproduced by any equilibrium counterpart.²⁸ Increasing

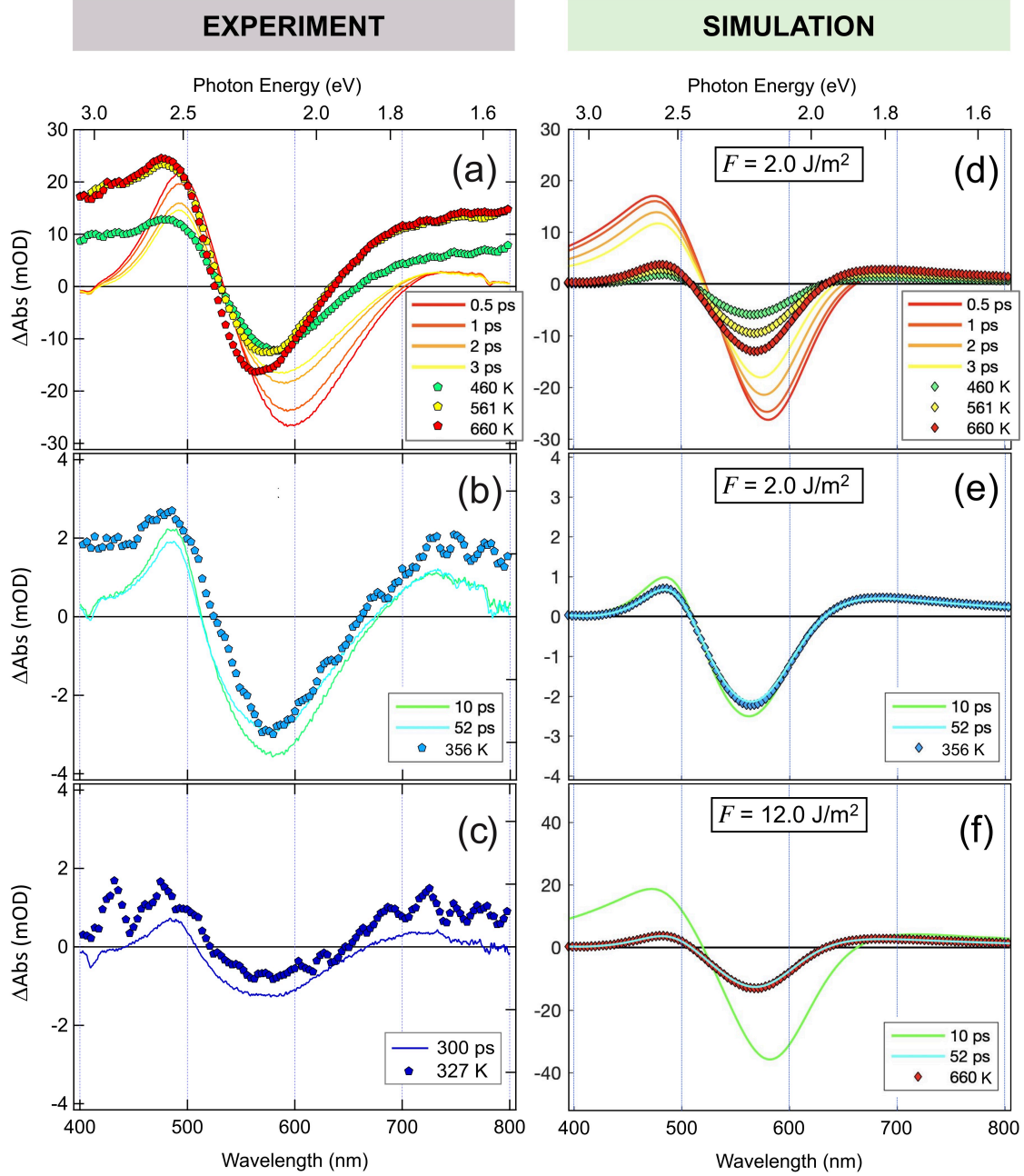


Figure 3: Comparison between static T_{bath} -dependent ΔAbs spectra (symbols) and delay-dependent dynamic TA spectra (lines). In panels (a), (b) and (c) are reported data for gradually-decreasing T_{bath} and gradually-increasing time delay τ , respectively. Panels (d) and (e) show numerical simulations corresponding to the experiments detailed in panels (a) and (b), respectively. Panel (f) reports on the theoretical study case with a pump fluence close to the damage threshold.

the delay and decreasing T_{bath} , the two sets of spectra gradually get more similar (Fig. 3(b), $\tau = 22 - 52 \text{ ps}$, $T_{bath} = 356 \text{ K}$), until they almost overlap, within experimental uncertainty (Fig. 3(c), $\tau = 300 \text{ ps}$, $T_{bath} = 327 \text{ K}$) .

In order to quantify the gradual rapprochement of static and dynamic data, we report in Fig. 4(a) the evolution of the PB-peak intensity *vs* its wavelength for different static T_{bath} (blue symbols) and delay time (red symbols) values (we do not report the experimental uncertainty for the sake of clarity). The trajectories of PB-peak evolution (visually highlighted by the dashed lines in Fig. 4(a)) lie very far apart from each other for high- T_{bath} /small- τ values, then become closer for $\tau \rightarrow 5 \text{ ps}$ and $460 \text{ K} > T_{bath} > 415 \text{ K}$, and start overlapping for $\tau \approx 10 \text{ ps}$ and $T_{bath} \approx 356 \text{ K}$. From there onwards, they follow the same path (green line) until the last recorded experimental points ($\tau = 300 \text{ ps}$, $T_{bath} = 327 \text{ K}$).

The increasing similarity between static and dynamic data for long- τ /low- T_{bath} is due to the achievement of thermodynamic equilibrium within the impulsively-excited system. Indeed, after few *ps*, $T_e = T_l$, and the heat diffusion to the substrate becomes the only significant ongoing process.^{14,29,49} At this stage, since LiF exhibits very low variations in refractive index with temperature,⁵⁰ the substrate heating is unlikely to have a significant effect on the overall plasmonic response. Thus the dynamic response for $\tau \geq 10 \text{ ps}$ is expected to be similar to the static response at aptly-chosen values of $T_{bath} > \text{RT}$. The small discontinuity in TAS data trend between the values at 5 ps and 10 ps is ascribed to NP breathing modes⁵¹ (clearly absent in static data).

The good overlap between dynamic and static data suggests the possibility to exploit the static T_{bath} data as an effective thermometric calibration for their dynamic counterpart. In order to do this, one can perform a linear fit across the low- T_{bath} static points (green line in Fig. 4(a)) and build an effective thermometric scale using the experimental static T_{bath} values as reference. Then, the experimental TA points can be projected onto the calibration line and, based on the position of the projection point, the dynamic temperature can be estimated. To do this, we chose to perform an orthogonal geometrical projection in the

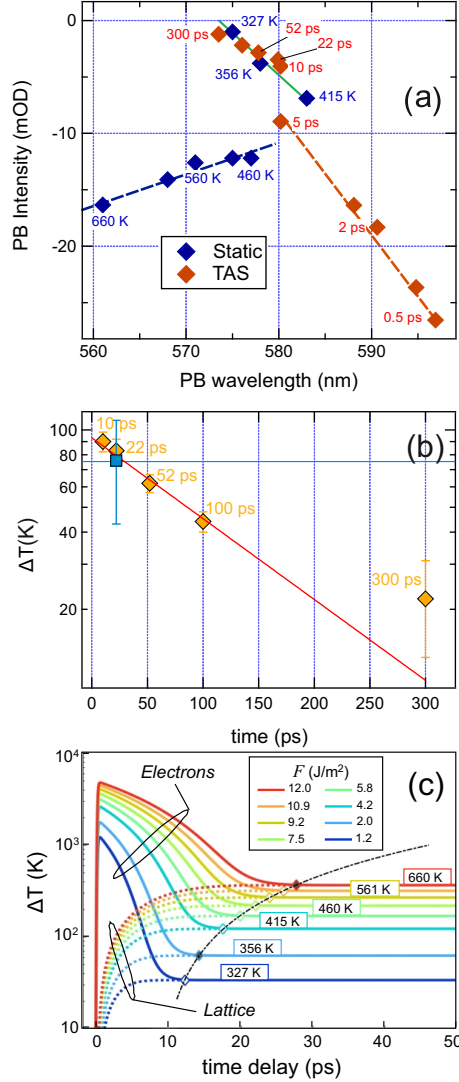


Figure 4: Panel (a): PB-peak intensity *vs* PB-peak wavelength extracted from dynamics TA spectra as a function of the delay time τ (red markers) or extracted from static T_{bath} -dependent data (blue markers). The values of τ and T_{bath} corresponding to each experimental point are reported in the graph. The dashed lines are a guide to the eye. The continuous green line is an interpolation of the static data in the (415-327) K T_{bath} interval. Panel (b): time dependence of the NP temperature extracted from the analysis of the data in panel (a) (orange symbols). Estimated low-delay NP temperature according to Eq. 1 (blue symbol). Exponential fit to the orange markers (red line). (c) Simulated electron (solid curves) and lattice (dashed curves) temperature dynamics after excitation with fs-laser pulses of increasing pump fluence. Diamonds mark the time delays τ_{EQ} of electron-lattice equilibration, with the cases corresponding to the simulations of Fig. 3(d)-(f) highlighted by gray filling. Dash-dot black line is a fitting ($R^2 = 0.9999$) power law $\tau_{EQ}(\Delta T_{max}) = a \times (\Delta T_{max})^{2/3} + b$, with $a = 0.385 \text{ ps K}^{-2/3}$, $b = 8.193 \text{ ps}$.

wavelength-intensity plane, meaning that the calibration temperature for a given TAS point corresponds to the value along the green line having the shortest distance from the point itself.

The result of this analysis, *i.e.* the delay-dependent temperature difference $\Delta T(\tau)$, with respect to RT, is reported in Fig. 4(b) (orange symbols). Treating the temperature evolution along the calibration line (*i.e.* the green line in Fig. 4(a)) as either a linear function, a polynomial function or an exponential curve, respectively, yields slightly different temperatures for the dynamic data, giving rise to the effective experimental uncertainty reported in Fig. 4(b). The $\Delta T(\tau)$ decay can be well fitted by means of an exponential function, as expected, yielding a time constant of $\alpha = (135 \pm 20)$ ps (red line). The agreement is quite good, save for the last data point, where the experimental uncertainty becomes larger due to the small magnitude of the experimental ΔAbs spectra.

In order to independently test the validity of such a thermometric calibration, we can independently evaluate the maximum laser-induced temperature increase of the NPs, ΔT_{max} according to Ref. 7. Under the hypothesis that the electromagnetic energy absorbed by the NP from the light pulse is used to homogeneously heat the NPs, that the dielectric function of Au is constant over the duration of the excitation pulse, and that no heat dissipation to the environment has occurred (an approximation valid within few tens of ps after the exciting pulse) ΔT_{max} can be expressed as:

$$\Delta T_{max} = \frac{\sigma_{abs} F}{V \rho_{Au} c_{Au}} \quad (1)$$

where V is the NP volume, ρ_{Au} and c_{Au} are the gold density and specific heat, F is the experimental laser fluence and σ_{abs} is the absorption cross section of a unit cell of the Au-NP array deduced from the calculations of Ref. 20. This implies that interparticle interaction effects in light-absorption are taken into account. Taking the experimental values $V = 4 \cdot 10^3 \text{ nm}^3$ and $F = (4 \pm 2) \text{ J/m}^2$, and taking $\sigma_{abs} = 2 \cdot 10^{-16} \text{ m}^2$,²⁰ we obtain $\Delta T_{max} = (75 \pm 30) \text{ K}$. This value is highlighted with a blue horizontal line in Fig. 4(b), intercepting

the thermometric calibration curve (red line) at around 20 ps time delay (blue symbol), in agreement with the experimental results of Fig. 3(b). Such a delay time can be interpreted as the lower limit of validity for a thermometric calibration in the considered TAS experiment, being the estimated ΔT_{max} representative of the NP temperature right after the electron-lattice equilibration.

To confirm this view, we resorted to numerical simulations of both thermal and TAS modulation experiments. For the plasmonic response of the nanostructures we adopted a simplified approach in which the individual nanoparticles are treated as isolated oblate nanoellipsoids in the quasi-static limit in a homogeneous environment with effective refractive index n_e .⁵² To mimick the red shift and broadening of the plasmonic resonance arising from interparticle couplings and inhomogeneities along the sample, we took n_e and the RT Drude damping constant of gold permittivity, Γ , as fitting parameters. The optical nonlinearity of gold was modeled according to the same approach reported in previous papers, including electronic and lattice heating effects being responsible to the subsequent modulation of interband and intraband permittivity contributions, respectively (see, *e.g.*, Ref. 33 and references therein for details). For the simulations of the static thermomodulation spectra, we simply assumed $T_l = T_e = T_{bath}$, whereas for the TAS simulations we employed the so-called three-temperature model,³³ to properly account for the electron and lattice temperature dynamics induced by pump absorption. The simulations confirm the general trend observed in the experiments in terms of a strong mismatch between the thermo-modulation spectra at high temperatures and the TAS spectra for moderately low pump fluence (around 2 J/m²) (Fig. 3(d)). Under this excitation condition, a good matching is instead retrieved between thermo-modulation spectra at intermediate temperatures and TAS spectra at around 10-20 ps time delay (Fig. 3(e)).

The simulations enabled us to explore the validity of a thermometric calibration also for very high pump fluences, approaching the damage threshold. Note that for 12 J/m² fluence the TAS spectrum well overlaps with the thermo-modulation spectrum at the highest tem-

perature (660 K), provided that a time delay of 40-50 ps is considered (Fig. 3(f)). Such a scaling of the time delay lower limit in the thermometric calibration is evidently connected to the electron-lattice equilibration which is expected to take more time for increasing pump fluence and thus for increasing ΔT_{max} .⁵³ This behavior is well captured by the numerical simulations of Fig. 4(c), where we have tracked the onset of electron-lattice equilibration by defying the time delay τ_{EQ} upon which $\Delta T_e(\tau_{EQ}) - \Delta T_l(\tau_{EQ}) \simeq 1 \times 10^{-2} \cdot \Delta T_l(\tau_{EQ})$ (diamonds in Fig. 4(c)).

The calibration procedure reported here is universal in the sense that its physical background lies in the photo-thermal response of Au, which is characteristic of the material only. Therefore, when changing the geometrical configuration of the nanostructures, both thermo-modulation and TAS spectra are modified in the same way, at least after $e-ph$ thermalization has occurred. The calibration reported in Fig. 4(b) is however not universally quantitatively exploitable because, whereas there is a unique way to perform thermo-modulation experiments, the heat deposited in a nanostructure will critically depend on its geometrical and dielectric parameters. Thus, for a given nanostructure, different pump wavelength or fluence, different quantities of heat can be deposited in the system, thereby modifying the electron heat capacity and the $e-ph$ thermalization time.

The agreement between the calibration curve and the temperature-rise estimate based on Eq. 1 implies that the amount of heat deposited in the NPs can be correctly assessed as the product of the fluence by the absorption cross section. According to our experimental values, we can therefore estimate the energy deposited on a single NP as $F \cdot \sigma_{abs} = (8 \pm 4) \cdot 10^{-16}$ J. Our method can be therefore fruitfully exploited to determine the amount of heat deposited in a nanostructure, a quantity often subject to large experimental uncertainties, albeit within the above-described general limits of applicability of the thermo-modulation calibration.

Conclusion

Summarizing, we have reported an approach for experimentally extracting a thermometric calibration scale of ultrafast processes based on the comparison of the dynamic plasmonic response of impulsively-excited Au plasmonic NPs with the corresponding static response as a function of temperature. Exploiting this method, we experimentally retrieved the evolution of the NP temperature as a function of the delay time τ . The results obtained with such a thermometric calibration were in good agreement with estimates of the NP temperature based on an independent model, confirming the soundness of the approach.

The method reported here is conceptually general, and applicable to all systems for which it is experimentally conceivable to measure the optical response following both ultrafast excitation and, separately, as a function of externally-controlled temperature. The application to plasmonic particles discussed here benefits from the resonant sensitivity of the optical response to the physical parameters of the material,⁵⁴ but the method is not limited to this kind of system. The thermometric calibration that we deduce provides a $T_{e,l}(\tau)$ curve that represents a highly-relevant input for all theoretical models of ultrafast relaxation dynamics and may help to explore fine details of the materials response to temperature under off-equilibrium conditions.

Supporting Information

Atomic force image of the Au NP array. Description of the experimental apparatus. Numerical model for the calculation of the static and dynamic plasmonic response. Comparison between experimental and calculated static and dynamic plasmonic response.

Acknowledgments

We acknowledge support from the Ministero dell’Istruzione, dell’Università e della Ricerca under the PRIN Grant 2015CL3APH and from the Compagnia di San Paolo (proj. Pan-Lab). This project has received funding from the European Union’s Horizon 2020 research and innovation programme under the Marie Skłodowska-Curie grant agreement N°799126. G.D.V. acknowledges partial support from the Ministero dell’Istruzione dell’Università e della Ricerca under the PRIN Grant 2015WTW7J3.

References

- (1) Voisin, C.; Del Fatti, N.; Christofilos, D.; Vallée, F. Ultrafast Electron Dynamics and Optical Nonlinearities in Metal Nanoparticles. *J. Phys. Chem. B* **2001**, *105*, 2264–2280.
- (2) Link, S.; El-Sayed, M. A. Optical Properties and Ultrafast Dynamics of Metallic Nanocrystals. *Ann. Rev. Phys. Chem.* **2003**, *54*, 331–366.
- (3) Hartland, G. V. Optical Studies of Dynamics in Noble Metal Nanostructures. *Chem. Rev.* **2011**, *111*, 3858–3887.
- (4) Hartland, G. V. Measurements of the Material Properties of Metal Nanoparticles by Time-Resolved Spectroscopy. *Phys. Chem. Chem. Phys.* **2004**, *6*, 5263–5274.
- (5) Jain, P. K.; Qian, W.; El-Sayed, M. A. Ultrafast Electron Relaxation Dynamics in Coupled Metal Nanoparticles in Aggregates. *J. Phys. Chem. B* **2006**, *110*, 136–142.
- (6) Feldstein, M. J.; Keating, C. D.; Liao, Y.-H.; Natan, M. J.; Scherer, N. F. Electronic Relaxation Dynamics in Coupled Metal Nanoparticles. *J. Am. Chem. Soc.* **1997**, *119*, 6638–6647.
- (7) Baffou, G.; Rigneault, H. Femtosecond-Pulsed Optical Heating of Gold Nanoparticles. *Phys. Rev. B* **2011**, *84*, 035415.

- (8) Baffou, G.; Quidant, R. Thermo-Plasmonics: Using Metallic Nanostructures as Nano-Sources of Heat. *Laser Photonics Rev.* **2013**, *7*, 171–187.
- (9) Taylor, A. B.; Siddiquee, A. M.; Chon, J. W. M. Below Melting Point Photothermal Reshaping of Single Gold Nanorods Driven by Surface Diffusion. *ACS Nano* **2014**, *8*, 12071–12079.
- (10) Herrmann, L. O.; Valev, V. K.; Tserkezis, C.; Barnard, J. S.; Kasera, S.; Scherman, O. A.; Aizpurua, J.; Baumberg, J. J. Threading Plasmonic Nanoparticle Strings with Light. *Nat. Commun.* **2014**, *5*, 4568.
- (11) González-Rubio, G.; Guerrero-Martínez, A.; Liz-Marzán, L. M. Reshaping, Fragmentation, and Assembly of Gold Nanoparticles Assisted by Pulse Lasers. *Acc. Chem. Res.* **2016**, *49*, 678–686.
- (12) Catone, D.; Ciavardini, A.; Di Mario, L.; Paladini, A.; Toschi, F.; Cartoni, A.; Fratoddi, I.; Venditti, I.; Alabastri, A.; Proietti Zaccaria, R.; O’Keeffe, P. Plasmon Controlled Shaping of Metal Nanoparticle Aggregates by Femtosecond Laser-Induced Melting. *J. Chem. Lett.* **2018**, *9*, 5002–5008.
- (13) Pustovalov, V. K. Light-to-Heat Conversion and Heating of Single Nanoparticles, Their Assemblies, and the Surrounding Medium under Laser Pulses. *RSC Adv.* **2016**, *6*, 81266–81289.
- (14) Brongersma, M. L.; Halas, N. J.; Nordlander, P. Plasmon-Induced Hot Carrier Science and Technology. *Nat. Nanotechnol.* **2015**, *10*, 25–34.
- (15) Bisio, F.; Principi, E.; Magnozzi, M.; Simoncig, A.; Giangrisostomi, E.; Mincigrucci, R.; Pasquali, L.; Masciovecchio, C.; Boscherini, F.; Canepa, M. Long-lived Nonthermal Electron Distribution in Aluminum Excited by Femtosecond Extreme Ultraviolet Radiation. *Phys. Rev. B* **2017**, *96*, 081119.

- (16) Halté, V.; Bigot, J.-Y.; Palpant, B.; Broyer, M.; Prével, B.; Pérez, A. Size Dependence of the Energy Relaxation in Silver Nanoparticles Embedded in Dielectric Matrices. *Appl. Phys. Lett.* **1999**, *75*, 3799–3801.
- (17) Stoll, T.; Maioli, P.; Crut, A.; Rodal-Cedeira, S.; Pastoriza-Santos, I.; Vallée, F.; Del Fatti, N. Time-Resolved Investigations of the Cooling Dynamics of Metal Nanoparticles: Impact of Environment. *J. Phys. Chem. C* **2015**, *119*, 12757–12764.
- (18) Manjavacas, A.; Liu, J. G.; Kulkarni, V.; Nordlander, P. Plasmon-Induced Hot Carriers in Metallic Nanoparticles. *ACS Nano* **2014**, *8*, 7630–7638.
- (19) Harutyunyan, H.; Martinson, A. B. F.; Rosenmann, D.; Khorashad, L. K.; Besteiro, L. V.; Govorov, A. O.; Wiederrecht, G. P. Anomalous Ultrafast Dynamics of Hot Plasmonic Electrons in Nanostructures with Hot Spots. *Nat. Nanotechnol.* **2015**, *10*, 770–774.
- (20) Magnozzi, M.; Proietti Zaccaria, R.; Catone, D.; O’Keeffe, P.; Paladini, A.; Toschi, F.; Alabastri, A.; Canepa, M.; Bisio, F. Interband Transitions Are More Efficient Than Plasmonic Excitation in the Ultrafast Melting of Electromagnetically Coupled Au Nanoparticles. *J. Phys. Chem. C* **2019**, *123*, 16943–16950.
- (21) Zhang, H.; Govorov, A. O. Optical Generation of Hot Plasmonic Carriers in Metal Nanocrystals: The Effects of Shape and Field Enhancement. *J. Phys. Chem. C* **2014**, *118*, 7606–7614.
- (22) Saavedra, J. R. M.; Asenjo-Garcia, A.; García de Abajo, F. J. Hot-Electron Dynamics and Thermalization in Small Metallic Nanoparticles. *ACS Photon.* **2016**, *3*, 1637–1646.
- (23) Magnozzi, M.; Ferrera, M.; Mattera, L.; Canepa, M.; Bisio, F. Plasmonics of Au Nanoparticles in a Hot Thermodynamic Bath. *Nanoscale* **2019**, *11*, 1140–1146.

- (24) Ferrera, M.; Magnozzi, M.; Bisio, F.; Canepa, M. Temperature-dependent permittivity of silver and implications for thermoplasmonics. *Phys. Rev. Materials* **2019**, *3*, 105201.
- (25) Plech, A.; Kotaidis, V.; Grésillon, S.; Dahmen, C.; von Plessen, G. Laser-Induced Heating and Melting of Gold Nanoparticles Studied by Time-Resolved X-ray Scattering. *Phys. Rev. B* **2004**, *70*, 195423.
- (26) Juvé, V.; Scardamaglia, M.; Maioli, P.; Crut, A.; Merabia, S.; Joly, L.; Del Fatti, N.; Vallée, F. Cooling Dynamics and Thermal Interface Resistance of Glass-Embedded Metal Nanoparticles. *Phys. Rev. B* **2009**, *80*, 195406.
- (27) Strasser, M.; Setoura, K.; Langbein, U.; Hashimoto, S. Computational Modeling of Pulsed Laser-Induced Heating and Evaporation of Gold Nanoparticles. *J. Phys. Chem. C* **2014**, *118*, 25748–25755.
- (28) Brown, A. M.; Sundararaman, R.; Narang, P.; Goddard, W. A.; Atwater, H. A. *Ab Initio* Phonon Coupling and Optical Response of Hot Electrons in Plasmonic Metals. *Phys. Rev. B* **2016**, *94*, 075120.
- (29) Pustovalov, V. K.; Smetannikov, A. S. Analytical and Computer Modelling of Thermal Processes of Laser Interaction with a Single Nanoparticle. *RSC Adv.* **2014**, *4*, 55760–55772.
- (30) Stoll, T.; Maioli, P.; Crut, A.; Del Fatti, N.; Vallée, F. Advances in Femto-Nano-Optics: Ultrafast Nonlinearity of Metal Nanoparticles. *Eur. Phys. J. B* **2014**, *87*, 260.
- (31) Labouret, T.; Palpant, B. Nonthermal Model for Ultrafast Laser-Induced Plasma Generation Around a Plasmonic Nanorod. *Phys. Rev. B* **2016**, *94*, 245426.
- (32) Brown, A. M.; Sundararaman, R.; Narang, P.; Schwartzberg, A. M.; Goddard, W. A.; Atwater, H. A. Experimental and *Ab Initio* Ultrafast Carrier Dynamics in Plasmonic Nanoparticles. *Phys. Rev. Lett.* **2017**, *118*, 087401.

- (33) Zavelani-Rossi, M.; Polli, D.; Kochtcheev, S.; Baudrion, A.-L.; Beal, J.; Kumar, V.; Molotokaite, E.; Marangoni, M.; Longhi, S.; Cerullo, G.; Adam, P.-M.; Della Valle, G. Transient Optical Response of a Single Gold Nanoantenna: The Role of Plasmon Detuning. *ACS Photon.* **2015**, *2*, 521–529.
- (34) Jermyn, A. S.; Tagliabue, G.; Atwater, H. A.; Goddard, W. A.; Narang, P.; Sundararaman, R. Transport of Hot Carriers in Plasmonic Nanostructures. *Phys. Rev. Materials* **2019**, *3*, 075201.
- (35) Block, A.; Liebel, M.; Yu, R.; Spector, M.; Sivan, Y.; García de Abajo, F. J.; van Hulst, N. F. Tracking Ultrafast Hot-Electron Diffusion in Space and Time by Ultrafast Thermomodulation Microscopy. *Sci. Adv.* **2019**, *5*, eaav8965.
- (36) Guillet, Y.; Charron, E.; Palpant, B. Spectral Dependence of the Ultrafast Optical Response of Nonspherical Gold Nanoparticles. *Phys. Rev. B* **2009**, *79*, 195432.
- (37) Wang, X.; Guillet, Y.; Selvakannan, P. R.; Remita, H.; Palpant, B. Broadband Spectral Signature of the Ultrafast Transient Optical Response of Gold Nanorods. *J. Phys. Chem. C* **2015**, *119*, 7416–7427.
- (38) Hobbs, R. G.; Putnam, W. P.; Fallahi, A.; Yang, Y.; Kärtner, F. X.; Berggren, K. K. Mapping Photoemission and Hot-Electron Emission from Plasmonic Nanoantennas. *Nano Lett.* **2017**, *17*, 6069–6076.
- (39) Lietard, A.; Hsieh, C.-S.; Rhee, H.; Cho, M. Electron Heating and Thermal Relaxation of Gold Nanorods Revealed by Two-Dimensional Electronic Spectroscopy. *Nat. Commun.* **2018**, *9*, 891.
- (40) Ortolani, M.; Mancini, A.; Budweg, A.; Garoli, D.; Brida, D.; de Angelis, F. Pump-Probe Spectroscopy Study of Ultrafast Temperature Dynamics in Nanoporous Gold. *Phys. Rev. B* **2019**, *99*, 035435.

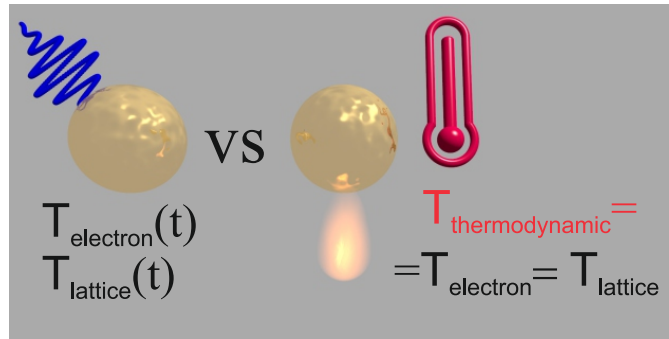
- (41) Van de Broek, B.; Grandjean, D.; Trekker, J.; Ye, J.; Verstreken, K.; Maes, G.; Borghs, G.; Nikitenko, S.; Lagae, L.; Bartic, C.; Temst, K.; Van Bael, M. J. Temperature Determination of Resonantly Excited Plasmonic Branched Gold Nanoparticles by X-ray Absorption Spectroscopy. *Small* **2011**, *7*, 2498–2506.
- (42) Plech, A.; Ibrahimkuty, S.; Reich, S.; Newby, G. Thermal Dynamics of Pulsed-Laser Excited Gold Nanorods in Suspension. *Nanoscale* **2017**, *9*, 17284–17292.
- (43) Anghinolfi, L.; Moroni, R.; Mattera, L.; Canepa, M.; Bisio, F. Flexible Tuning of Shape and Arrangement of Au Nanoparticles in 2-Dimensional Self-Organized Arrays: Morphology and Plasmonic Response. *J. Phys. Chem. C* **2011**, *115*, 14036–14043.
- (44) Proietti Zaccaria, R.; Bisio, F.; Das, G.; Maidecchi, G.; Caminale, M.; Vu, C. D.; De Angelis, F.; Di Fabrizio, E.; Toma, A.; Canepa, M. Plasmonic Color-Graded Nanosystems with Achromatic Subwavelength Architectures for Light Filtering and Advanced SERS Detection. *ACS Appl. Mater. Interfaces* **2016**, *8*, 8024–8031.
- (45) Sugawara, A.; Mae, K. Surface Morphology of Epitaxial LiF(110) and CaF₂(110) layers. *J. Vac. Sci. Tech. B* **2005**, *23*, 443–448.
- (46) Fratoddi, I. et al. Gold Nanoparticles Functionalized by Rhodamine B Isothiocyanate: A New Tool to Control Plasmonic Effects. *J. Coll. Interf. Sci.* **2018**, *513*, 10 – 19.
- (47) Doremus, R. H. Optical Properties of Small Gold Particles. *J. Chem. Phys.* **1964**, *40*, 2389–2396.
- (48) Yeshchenko, O.; Bondarchuk, I.; Gurin, V.; Dmitruk, I.; Kotko, A. Temperature Dependence of the Surface Plasmon Resonance in Gold Nanoparticles. *Surf. Sci.* **2013**, *608*, 275 – 281.
- (49) Della Valle, G.; Conforti, M.; Longhi, S.; Cerullo, G.; Brida, D. Real-Time Optical

- Mapping of the Dynamics of Nonthermal Electrons in Thin Gold Films. *Phys. Rev. B* **2012**, *86*, 155139.
- (50) Li, H. H. Refractive Index of Alkali Halides and its Wavelength and Temperature Derivatives. *J. Phys. Chem. Ref. Data* **1976**, *5*, 329.
- (51) Hodak, J. H.; Martini, I.; Hartland, G. V. Observation of Acoustic Quantum Beats in Nanometer Sized Au Particles. *J. Chem. Phys.* **1998**, *108*, 9210–9213.
- (52) Silva, M. G.; Teles-Ferreira, D. C.; Siman, L.; Chaves, C. R.; Ladeira, L. O.; Longhi, S.; Cerullo, G.; Manzoni, C.; de Paula, A. M.; Della Valle, G. Universal Saturation Behavior in the Transient Optical Response of Plasmonic Structures. *Phys. Rev. B* **2018**, *98*, 115407.
- (53) Hodak, J.; Martini, I.; Hartland, G. V. Ultrafast Study of Electron–Phonon Coupling in Colloidal Gold Particles. *Chem. Phys. Lett.* **1998**, *284*, 135–141.
- (54) Kelly, K. L.; Coronado, E.; Zhao, L. L.; Schatz, G. C. The Optical Properties of Metal Nanoparticles: The Influence of Size, Shape, and Dielectric Environment. *J. Phys. Chem. B* **2003**, *107*, 668–677.

Thermometric Calibration of the Ultrafast Relaxation Dynamics in Plasmonic Au Nanoparticles

Marzia Ferrera, Giuseppe Della Valle, Maria Sygletou, Michele Magnozzi, Daniele Catone,
Patrick O’Keeffe, Alessandra Paladini, Francesco Toschi, Lorenzo Mattera, Maurizio
Canepa, Francesco Bisio

We compare the dynamic optical response of plasmonic Au nanoparticles following ultrashort-pulse excitation with their static optical response as a function of increasing temperature. From this comparison, the optical fingerprints of equilibrium or off-equilibrium state can be clearly identified, allowing to extract a dynamic thermometric calibration scale of the relaxation process.



Graphical Table of Contents